Effect of Deep-Space Temperature on Lithium-Ion Battery Transport

Final Report

Megan Darby

Introduction

Following earthbound energy storage trends, Lithium-Ion batteries (LIB) have become the dominating battery chemistry for aerospace and space exploration replacing previous chemistries like Nickel Metal Hydride (1). Applications include powering International Space Station spacesuits, providing external power for telecommunication satellites when solar power is lost, or powering Entry, Descent, and Launch (EDL) operations and surface operations on a deep-space craft like the Mars Exploration Rovers (1) (2). When expanding the applications of LIBs, performance at low temperatures becomes a concern. As Ma et al. described, at very low temperatures like less than 0°C, LIB performance degrades due to several different factors like an increase in electrolyte viscosity (decreasing ionic conductivity), slower diffusion of Li^+ions, and increased charge transfer resistance (3). This study's objective is to vary the initial temperature of a $LiCoO_2$ (LCO) battery with a graphite anode and $LiPF_6$ -based electrolyte operating on Mars and determine its effect on battery charge and discharge performance.

Model Formulation

A numerical model of the temperature change of an LCO cell operating on Mars was developed to study the effect of initial temperature on performance. The device under study is a single prismatic Lithium Ion cell traveling on Mars' surface; the geometry below is representative of cells that are connected in parallel to create batteries used on the Mars Rover programs (Figure 1) . In the model the cell is operated at a C-rate $C/5$, taken from the low-temperature acceptance testing requirements in the Mars exploration battery study (2). Table 1 summarizes key geometry and material properties for each region of the cell. Most material properties were estimated for the model at the average value of the initial temperature test values.

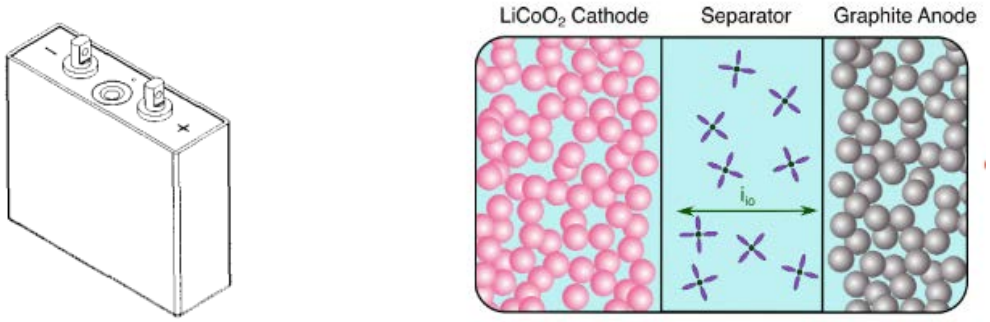

Figure 1. Lithium Ion prismatic cell geometry (Left) (2) and internal cell chemistry (Right) (4)

Table 1: Cell Geometry and Material Properties

	Anode – Graphite	Separator	Cathode - LCO	Value Source
Thickness [m]	66E-6	20E-6	58E-6	(5)
Volume fraction	0.65	0.65	0.65	
Density [kg/m^3]	1060	1132	1540	(5)
Capacity [Ah/kg]	370	-	140	(6)
Specific Heat [J/kg-K]	688.10	1453.43	613.70	(7) (7) (8)
Thermal Conductivity [W/m-K]	1.40	0.10	0.50	(9)

The model is a 1D Single Particle Model (SPM) approximation for a cell, which neglects radial and spatial gradients and assumes all particles within an electrode are the same size and change consistently. This allows the state of all particles in an electrode to be modeled by the changes in a single particle (10). The model calculates volumetric heat transfer modes and thermal energy generation terms in each of the cell regions— the anode, separator, and cathode respectively, in order to solve for the dynamic temperature of the cell. The model is discretized with 1 node for each region of the cell. Equation 1 shows the energy balance on a cell region (4):

$$\frac{dT_{region}}{dt} = \frac{1}{\rho C_p}\left[\dot{Q}'''_{rad} + \dot{Q}'''_{cond,i} - \dot{Q}'''_{cond,e} + \dot{Q}'''_{conv} + \dot{Q}'''_{ohm,el} + \dot{Q}'''_{ohm,io} + \dot{Q}'''_{rxn}\right] \quad [1]$$

$\dot{Q}'''_{rad}$ captures the effect of radiation heat transfer from the external environment to the battery cell; $\dot{Q}'''_{cond}$ is the conduction heat transfer between elements in the cell, which typically includes an entering and exiting term; $\dot{Q}'''_{conv}$ is the convection heat transfer between the external environment and cell; $\dot{Q}'''_{ohm}$ is the heat generation due to ionic and electrical resistance; and $\dot{Q}'''_{rxn}$ accounts for heat generated by chemical reactions at the interfaces or bulk of the cell regions. Not all regions of the cell experience the same heat generation phenomena; for instance, both radiation and convection only affect the boundaries of the cell (anode and cathode), while the separator is inert with no electrical resistance and no internal reactions so $\dot{Q}'''_{ohm,el}$ and $\dot{Q}'''_{rxn}$ are both zero . Bulk reactions for all regions were neglected for this model.

The volumetric heat generation due to interfacial reactions in the anode and cathode is found using Equation 2, where $\dot{s}_k$ is the molar production rate depending on interfacial charge transfer reactions and e_k is each species thermodynamic and electrical energy. Additionally, due to charge neutrality required by the SPM, ionic current and electric current are equivalent to the external current applied to the cell, so both ohmic heat generation terms can be described by Equation 3 with respective material resistivity, R .

$$\dot{Q}'''_{rxn} = -\sum_k \dot{s}_k e_k \quad [2] \qquad \dot{Q}'''_{ohm,io\ or\ el} = i_{ext}^2 R_{io\ or\ el} \quad [3]$$

Figure 2 shows a representative diagram of the thermal processes at the cell electrodes.

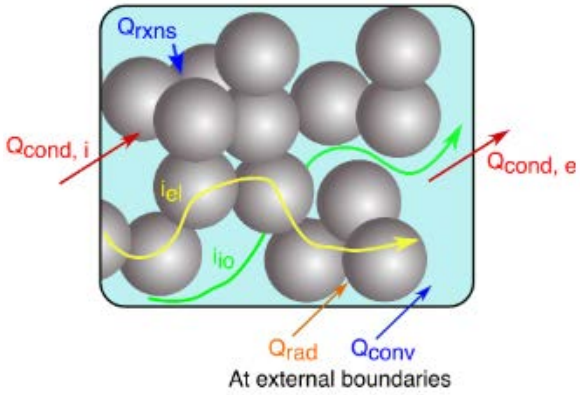

Figure 2. Electrode thermal processes (4)

For heat transfer parameters in the model, the emissivity of the battery cell was assumed to be 0.75 [ ], while the convection heat transfer coefficient, h_c, was averaged from a CFD study on wind and thermal activity on the planet's surface; assuming wind speeds at 4 m/s , the coefficient is 6.303 W/m^2-K (11).

Note that this model can only be an initial estimation of cell temperature and does not evaluate cell charge and discharge performance. There are some parallel phenomena neglected in the model that would modify the temperature evolution. For instance, parameters assumed as fixed such equilibrium double layer potential should be calculated via the Nernst equation to consider species activity, Gibb's energy, and temperature effects. The changing equilibrium double layer potential affects the overpotential and charge transfer kinetics at each cell electrode via the Butler-Volmer expression for faradaic current. Additionally, no species balance equations are included in the model which hamper its physical accuracy.

Results and Discussion

Using the modeling approach discussed, dynamic temperature plots were developed for the LCO cell. The temperature of the anode, separator, and cathode collapsed on each other, displaying the same temperature profile; this result is due to the small thicknesses of each region (micron-scale) (Figure 3). Without additional outside influence, e.g., an external heater, the cell temperature will cool towards and stabilize to right above the ambient surroundings, 210.414 K (-62.74◦C). This is not an optimum temperature for continuous operation, so cells are often packaged in an insulated electronics box in tandem with resistive heaters to keep the cell temperature higher on exploration spacecraft (2).

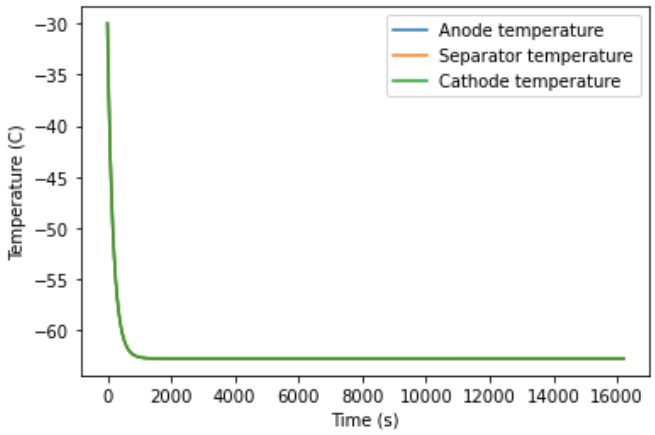

Figure 3. Dynamic temperature in cell anode, separator, and cathode for initial temperature -30°C

This behavior takes a varying amount of time depending on the initial temperature value (T_0). For instance, the case starting at ambient Mars conditions (-62.78 ◦C) takes approximately 0.28 hours to reach its steady state temperature, while the warmest case (0 ◦C) takes 0.57 hours to reach steady state. The time required to reach steady state is shown more clearly for each T_0 case in Figure 4.

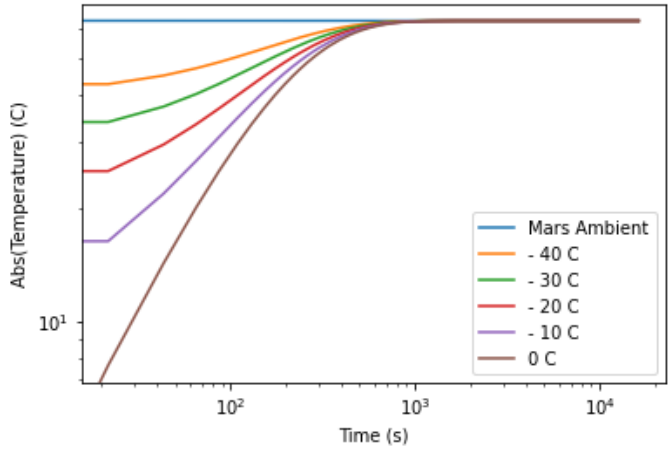

Figure 4. Time to steady-state for tested initial temperatures

Conclusion

This study investigated the effect of varying initial temperature for an LCO cell's dynamic temperature balance in Mar's ambient conditions. Due to the geometry of the cell, there is no significant temperature difference internally, and all initial temperatures tested stabilized at just above ambient temperature conditions, -62.74◦C. This indicates that the volumetric heat generation terms will not provide significant temperature difference for the battery cell by itself (less than ~0.1◦C) and external heaters are necessary to reach more optimum operating temperatures for this model. This model is heavily limited by unexplored parallel phenomena, such as temperature's impact on the changing equilibrium potentials and species consumption balance.

References

1. Nobel-winning lithium-ion batteries powering space. *The European Space Agency.* [Online] 2019. https://www.esa.int/Enabling_Support/Space_Engineering_Technology/Nobel-winning_lithium-ion_batteries_powering_space.

2. *Lithium Ion Batteries on 2003 Mars Exploration Rover.* Bugga, Ratnakumar, et al. Huntsville, AL : NASA Battery Workshop, 2002.

3. *Temperature effect and thermal impact in lithium-ion batteries: A review.* Ma, Shuai, et al. 6, s.l. : Progress in Natural Science: Materials International, Vol. 28.

4. Decaluwe, Steven. Lecture 25 - Conservation Equations for Energy. *MEGN 570 - Electrochemical Systems Engineering .* 2020.

5. Chang, Wesley, et al. Understanding Adverse Effects of Temperature Shifts on Li-Ion. *Journal of The Electrochemical Society.* 2020. Vol. 167.

6. *Current Li-Ion Battery Technologies in Electric Vehicles and Opportunities for Advancements.* Miao, Yu, et al. s.l. : Energies, 2019, Vol. 12.

7. Linstrom, P.J. and Mallard, W.G. *NIST Chemistry WebBook , NIST Standard Reference Database Number 69.* s.l. : National Institute of Standards and Technology, 2018. https://doi.org/10.18434/T4D303.

8. *New experimental heat capacity and enthalpy of formation of lithium cobalt oxide.* Gotcu-Freis, Petronela, et al. s.l. : The Journal of Chemical Thermodynamics, 2015, Vol. 84.

9. *Characterization of thermal conductivity and thermal transport in lithium-ion battery .* Marconnet, Amy, Kantharaj, Rajath and Sun, Yexin. Houston, TX : NASA Thermal & Fluids Analysis Workshop, 2018.

10. Decaluwe, Steven. Lecture 17- Conservation of Charge and Bulk Species in Batteries. *MEGN 570 - Electrochemical Systems Engineering.* 2020.

11. *Convective Heat Transfer Measurements at the Martian Surface.* Soria-Salinas, A., Zorzano, M.-P, and Martin-Torres, J. s.l. : Symposium on Space Educational Activities, 2015.